The finite length diocotron mode

K. S. Fine and C. F. Driscoll[a]

Physics Department and Institute for Pure and Applied Physical Sciences, University of California at San Diego, La Jolla, California 92093

A simple model is presented of a finite length electron plasma column supporting a small amplitude diocotron wave with mode number $m=1$. The electrons are contained inside conducting cylinders in an axial magnetic field, with negative voltages on end cylinders providing axial containment. The $m=1$ diocotron mode is the $\mathbf{E}\times\mathbf{B}$ drift orbit of an offset electron column around the cylinder axis, due to radial electric fields from image charges on the wall. The model predicts that the mode frequency will be higher than that of an infinitely long column due to θ-drifts from the radial containment fields at the plasma ends. The predicted dependencies on plasma length, radius, and temperature agree well with experiments, where frequency increases up to $2.5\times$ are observed. For very short plasmas, these containment fields predominate over the image charge fields, and the plasma orbit is called the ''magnetron'' mode. The shift in the magnetron frequency due to image charges is also calculated. © *1998 American Institute of Physics.* [S1070-664X(98)02303-9]

I. INTRODUCTION

Small amplitude diocotron modes are ''surface'' waves on magnetized electron columns inside conducting cylinders,[1,2] with density perturbations $\delta n(r)\exp[i(m\theta-k_z z-\omega t)]$. The mode with $m=1$ and $k_z\approx 0$ is particularly simple, since it is just a displacement of the column off center. This mode is fundamental to manipulation and control in charged particle traps, and also is easily measured and useful as a nondestructive diagnostic of the electron plasma.

For long columns, the $m=1$ mode is understood as an $\mathbf{E}\times\mathbf{B}$ drift orbit resulting from the electric field arising from the *image charges* in the conducting wall. Alternately, for small, ellipsoidal charge clouds, the mode is thought of as a drift arising from the radial component of the end *confinement* fields, and is usually called the ''magnetron'' mode.[3] For finite length columns, both image and confinement electric fields are present, and we present a model which includes both. Furthermore, we have compared the predicted frequency of this model to experiments, and find good agreement for columns with lengths longer than the diameter of the containment cylinders. In addition, the model also predicts a significant variation of the mode frequency with plasma temperature, which has also been verified by experiments. Finally, we present a calculation of the correction to the magnetron mode of an ellipsoidal cloud due to image charges in the cylindrical walls.

II. EXPERIMENTAL GEOMETRY

A schematic diagram of a typical experiment is shown in Fig. 1. A uniform axial magnetic field $B\hat{z}$ provides radial confinement, and negative voltages applied to end cylinders A and C confine the electrons axially. By varying the number of cylinders in the containment region B, we can vary the

confined plasma length over the range $2\leq L_p\leq 36$ cm. The cylinders have a uniform wall radius of $R_w=3.81$ cm.

The apparatus is operated in an inject–manipulate–dump cycle. For injection, cylinder A is briefly grounded, allowing electrons to enter from the negatively biased thermionic source. The trapped electron column can then be manipulated, and waves can be transmitted and received using sector probes, which are electrically isolated sections of the wall. Finally, the column is dumped by grounding cylinder C: The electrons stream out along the magnetic field lines, and measurement of the charge which passes through a moveable collimator hole gives the z-integrated electron density $Q_z(r,t)$, which is related to the previously confined density $n(r,z,t)$ by

$$\frac{Q_z(r,t)}{-eA_h}=\int n(r,z,t)dz,\tag{1}$$

where $A_h=\pi(0.16\text{ cm})^2$ is the area of the collimator hole. The charge on the endplate is also measured, so that the total number of electrons in the column, N_{tot}, is known.

The plasmas studied here have electron density in the range $10^6\leq n\leq 10^7$ cm^{-3}, thermal energy $0.4\leq T\leq 4$ eV, radii $0.95\leq R_p\leq 2.8$ cm, and magnetic fields $100\leq B\leq 400$ Gauss. For these parameters, the individual electrons bounce rapidly along the magnetic field, $B\hat{z}$, and the electrons $\mathbf{E}\times\mathbf{B}$ drift more slowly around the plasma axis. We will assume that the bounce frequency, $\nu_b\equiv\bar{v}/2L_p$, is large compared to the rotation frequency, $\nu_r=2\pi nec/B$. The experiments presented here lie in the range $2\leq\nu_b/\nu_r\leq 80$. In the model, we assume that ν_b/ν_r is large, so that the dynamics of the plasma will be that of a collection of essentially ''rigid'' charged rods which move in (r,θ) due to $\mathbf{E}\times\mathbf{B}$ drifts in the electric field from all the other charged rods.

For such a rigid column, the $m=1$ diocotron mode has a simple interpretation; it is simply a displacement of the column from the cylinder axis. The resulting image charges in
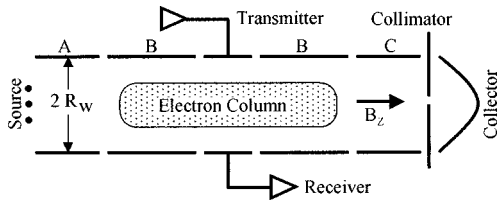
FIG. 1. Schematic diagram of the cylindrical containment apparatus.

the wall then create a radial electric field which causes the column to drift around the cylinder axis. In the next section we review the simple theory for this mode for a column with no ends.

III. INFINITE LENGTH THEORY

Figure 2 shows an end view of an electron column offset from the cylinder axis by distance $D\hat{x}$. Assume that the column is infinite in length, cylindrically symmetric about its axis, and has charge per unit length of $-Ne$, where the "line density" is $N \equiv \int 2\pi r\,dr\,n(r) \approx \pi R_p^2 n$. From Gauss' Law, the electric field outside such a column is identical to the field of a single line charge located at the column center and also having charge $-Ne$ per unit length. Therefore, the image field is the same, and is known to be equal to that of a line charge of $+Ne$ charge per unit length located at radius R_w^2/D. For $D/R_w \ll 1$, the field from this image charge at the column is a uniform electric field in the $-\hat{x}$ direction of magnitude

$$E_i = \frac{2Ne}{R_w^2/D}. \tag{2}$$

This radial image charge field causes an $\mathbf{E} \times \mathbf{B}$ drift in the $\hat{\theta}$ direction, and the column orbits around the trap axis at a frequency

$$f_\infty = \frac{cNe}{\pi B R_w^2}. \tag{3}$$

Note that this frequency is independent of the radial density profile of the column, and independent of the offset D. Thus, the uniform electric field causes the column to orbit around the cylinder axis, with no other density changes. This simple result for the infinite length $m=1$ mode was first noted by Levy.[4]

However, when D becomes large, the image charge comes closer to the column, and the electric field variations
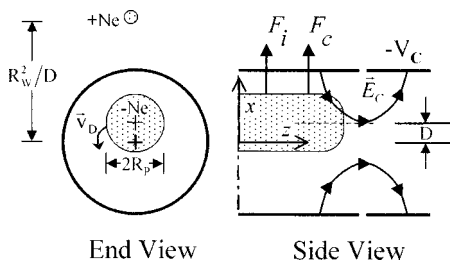

FIG. 2. Two views of an offset electron column: an end view and a side view of one of the column ends.

across the column become significant. This problem has been solved to order $(D/R_w)^2$ for constant density columns,[5] and the result is that the column distorts into an elliptical cross-section with the long elliptical axis pointed along the $\hat{\theta}$ direction of motion. This nonlinear distortion causes an amplitude dependence of the mode frequency, given by

$$f_{\mathrm{NL}} = f_\infty + f_\infty \left(\frac{1 - 2(R_p/R_w)^2}{[1 - (R_p/R_w)^2]^2} \right) \left(\frac{D}{R_w} \right)^2. \tag{4}$$

This nonlinear frequency shift has been recently obtained analytically for more general density profiles.[6] In the finite length model presented in the following section, we will ignore terms of order (D/R_w) and higher. However, when we compare this model to experiment, we will need to correct for this quadratic variation of mode frequency with amplitude, since the experiments are performed at finite amplitude.

IV. FINITE LENGTH MODEL

Equation (3) suggests that the $m=1$ mode frequency can be used as a nondestructive measure of N. However, if both N and the $m=1$ frequency f are measured in an experiment, it is found that f is significantly larger than f_∞, sometimes by as much as a factor of two or three.

This frequency increase is caused by the extra forces from the containment fields. This is illustrated in the side view in Fig. 2. The infinite length theory includes only the force F_i due to the images acting in the $+x$ direction. However, there is also a force F_c in the $+x$ direction due to the containment fields. Like the image force F_i, the containment force F_c is proportional to D/R_w. This containment force F_c is localized at the ends of the column, but the $m=1$ frequency can be calculated from the $\mathbf{E} \times \mathbf{B}$ drift due to the total z-integrated force in the x direction, $F_{\mathrm{tot}} = F_i + F_c$, as

$$f = \frac{cF_{\mathrm{tot}}}{(-N_{\mathrm{tot}}e)B2\pi D}, \tag{5}$$

where $-N_{\mathrm{tot}}e$ is the total column charge. We ignore the column's self electric fields, since the self forces cancel from Newton's 3$^{\mathrm{rd}}$ Law.

We are assuming that the column is *rigid*; that is, that the bounce frequency of electrons along the magnetic field is large compared to drift motions perpendicular to the magnetic field. This bouncing averages over the z variations of the containment force. Such a column will behave as if composed of a collection of rigid rods, each rod being an individual electron. When moved off axis, each rod will remain straight and aligned with the magnetic field. This is the *opposite* to the assumption made in a previous paper by Prasad and O'Neil,[7] where the bounce frequency was assumed small, and the columns could bend.

In addition, we ignore density changes at the ends of the column. These density changes come about because the confinement fields are different at the off-axis position, so that the length of the rigid rods will change. This effect is the origin of "rotational pumping," which causes damping of the $m=1$ mode.[8] We find that the frequency corrections due to these density changes vary as $(R_p/R_w)^2$, which we will ignore for this analysis.

Finally, we make the experimentally reasonable assumptions that the applied end confinement voltage V_c is much greater than the plasma potential, i.e. $V_c \gg |\Phi_p|$, and that the column is fairly long, i.e. $L_p \gg R_w$. The first condition implies that the end of the column is far from the containment cylinder, so that we can approximate the z-variation of the containment field as

$$E_{zc} \propto e^{\pm j_{01}z/R_w}, \tag{6}$$

where $j_{01} = 2.405$ is the first zero of the J_0 Bessel function, and the minus sign applies to the left containment cylinder.

We first calculate the containment force F_c. When the column is on axis, the net containment force on one end is only in the z direction. When the column is displaced off-axis, one end will have in addition a force in the x direction:

$$F_{xc}^1 = \int_{\text{One End}} d^3x(-en_0)\delta E_{xc}, \tag{7}$$

where $n_0(r,z)$ is the density when the plasma is on-axis, and $\delta E_{xc}(r,z)$ is the change in containment electric field due to the column being off axis. The superscript 1 indicates force on one end only. For small D

$$\delta E_{xc} \approx D\frac{\partial E_{xc}}{\partial x} = -D\left(\frac{\partial E_{yc}}{\partial y} + \frac{\partial E_{zc}}{\partial z}\right), \tag{8}$$

where Laplace's equation has been used. Combining these two expressions, we have

$$F_{xc}^1 = D\int_{\text{One End}} d^3x\ en_0\left(\frac{\partial E_{yc}}{\partial y} + \frac{\partial E_{zc}}{\partial z}\right). \tag{9}$$

From symmetry, the first term on the right hand side is just equal to $-F_{xc}^1$, so

$$F_{xc}^1 = \frac{1}{2}D\int d^3x\ en_0\frac{\partial E_{zc}}{\partial z}. \tag{10}$$

Next, we make use of Eq. (6) to obtain

$$\frac{\partial E_{zc}}{\partial z} \approx -\frac{j_{01}}{R_w}E_{zc}. \tag{11}$$

Combining these last two expressions, we have

$$F_{xc}^1 = \frac{1}{2}\frac{j_{01}}{R_w}D\int_{\text{One End}} d^3x(-en)E_{zc}. \tag{12}$$

We recognize the integral as the containment force on one end in the z direction, F_{zc}^1, so that including both ends, the total containment force in the x direction is

$$F_c = 2F_{xc}^1 = D\frac{j_{01}}{R_w}F_{zc}^1. \tag{13}$$

The containment force from one end must balance the pressure and electric forces across the $z=0$ plane that bisects the column (see Fig. 2). Integrating over this plane gives

$$F_{zc}^1 = \int_{z=0} dA\left(n_0T + \frac{E^2}{8\pi}\right). \tag{14}$$

We evaluate this integral for a uniform density profile, and assume that the column length is long enough so that the electric field at $z=0$ is the same as for an infinite column. We find that only the line density N enters, as

$$F_{zc}^1 = NT + N^2e^2\left(\frac{1}{4} + \ln\frac{R_w}{R_p}\right), \tag{15}$$

where T is the electron temperature. Inserting this result back into Eq. (13), we now have an expression for the total containment force:

$$F_c = D\frac{j_{01}}{R_w}\left[NT + N^2e^2\left(\frac{1}{4} + \ln\frac{R_w}{R_p}\right)\right]. \tag{16}$$

Next, we calculate the image force, F_i, on a finite length column. For a length L_p of an infinite length column, the total image force in the x direction would be

$$F_{i\infty} = (-Ne)\frac{-2Ne}{R_w^2/D}L_p = 2N^2e^2\left(\frac{D}{R_w}\right)\left(\frac{L_p}{R_w}\right). \tag{17}$$

If this force is used in Eq. (5), we will recover the infinite length frequency, f_∞. For a finite length column, F_i will be somewhat smaller than this, because the fields from the images will spread at the column ends. It is easiest to calculate what will be *missing* from $F_{i\infty}$ for a finite length column.

Suppose we divide an infinite length, off-axis column into two pieces: one part from from $z=0$ to $z=-\infty$, another from $z=0$ to $z=+\infty$. Let us calculate ΔF_{xi}^1, the force in the x direction of the images of the left column acting on the right column. This force, times two for each end, will be subtracted from $F_{i\infty}$ to find the image force.

To do this calculation we use the Green's function for charges in a grounded, conducting cylinder in cylindrical coordinates:[9]

$$G(\mathbf{x},\mathbf{x}') = \frac{4}{\pi}\int_0^\infty dk\ \cos k(z-z')$$

$$\times\left[\begin{array}{l}\left(\frac{1}{2}I_0(kr_<)K_0(kr_>) + \sum_{m=1}^\infty I_m(kr_<)K_m(kr_>)\cos m(\theta-\theta')\right) \\ -\left(\frac{1}{2}\frac{K_0(kR_w)}{I_0(kR_w)}I_0(kr_<)I_0(kr_>) + \sum_{m=1}^\infty \frac{K_m(kR_w)}{I_m(kR_w)}I_m(kr_<)I_m(kr_>)\cos m(\theta-\theta')\right)\end{array}\right], \tag{18}$$

where I and K are the modified Bessel functions, and $r_>(r_<)$ indicate the larger (smaller) radius of the source and field points. The second term in the large brackets is due to the image charges; note that only this term depends upon the wall radius. To calculate the field of the images alone, we separate out this term, defining the image Green's function, $G_i(\mathbf{x},\mathbf{x}')$.

Next, we reduce the two columns to two half infinite line charges. There are two approximations here. The finite column size will have corrections to order $(R_p/R_w)^2$ and higher, which we ignore for this analysis. In addition, the actual column ends are not flat, but are rounded. With these approximations, the potential due to the images of a line charge extending from $z=-\infty$ to $z=0$ and off-axis in the x direction by D, can be found by integrating over $G_i(\mathbf{x},\mathbf{x}')$:

$$\phi_i(r,\theta,z) = \int_{-\infty}^{0} dz' \int dr' \int r'\,d\theta'(-eN)\delta(\theta')$$

$$\times \frac{\delta(r'-D)}{D}G_i(\mathbf{x},\mathbf{x}')$$

$$\approx \frac{\phi_{i\infty}}{2} - \frac{4eN}{\pi}\int_0^\infty dk\,\frac{\sin kz}{k}$$

$$\times\left[\frac{1}{2}\frac{K_0(kR_w)}{I_0(kR_w)}I_0(kr)I_0(kD)\right.$$

$$\left. + \frac{K_1(kR_w)}{I_1(kR_w)}I_1(kr)I_1(kD)\cos\theta\right]. \tag{19}$$

Here, $\phi_{i\infty}$ is the potential of an infinite length column, and we have eliminated all terms of order $(D/R_w)^2$ and greater. Now we calculate ΔF_{xi}^1 for a column at $\theta=0$:

$$\Delta F_{xi}^1 = \int_0^\infty dz(-Ne)\frac{\partial\phi_i}{\partial r}. \tag{20}$$

Using Eq. (19) for ϕ_i, along with the small argument expansions for I_0 and I_1, we find after some variable substitutions:

$$\Delta F_{xi}^1 = \frac{N^2e^2D}{R_w}\lim_{b\to\infty}\left[b - \frac{1}{\pi}\int_0^\infty du\left(\frac{K_0(u)}{I_0(u)}+\frac{K_1(u)}{I_1(u)}\right)\right.$$

$$\left. \times(1-\cos ub)\right]. \tag{21}$$

The above expression can be evaluated numerically to find

$$\Delta F_{xi}^1 = 0.671\frac{N^2e^2D}{R_w}, \tag{22}$$

and we use this expression to finally obtain the image force:

$$F_i = F_{i\infty}\left(1 - 0.671\frac{R_w}{L_p}\right). \tag{23}$$

For large L_p, the image force approaches the result for an infinite column, as expected.

Finally, we can calculate the (small amplitude) finite length frequency f of the mode with corrections due to the end confinement fields and due to the reduced image charge force:
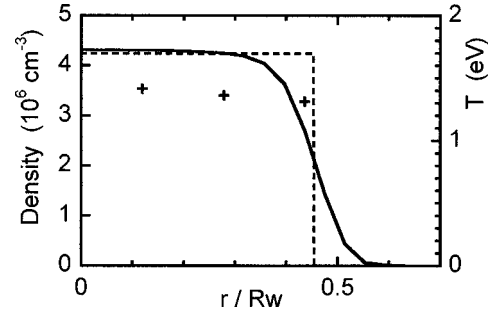

FIG. 3. Measured density profile with $R_p/R_w=0.45$ (solid line). Also shown are the measured temperatures (plusses) and the model profile used in our model calculations (dashed line).

$$\frac{f}{f_\infty} = \frac{F_{\text{tot}}}{F_{i\infty}} = \frac{F_c+F_i}{F_{i\infty}}$$

$$= 1 + \left[\frac{j_{01}}{2}\left(\frac{1}{4}+\ln\frac{R_w}{R_p}+\frac{T}{Ne^2}\right)-0.671\right]\left(\frac{R_w}{L_p}\right). \tag{24}$$

Note that for a uniform density column, the temperature term can be approximated as $T/Ne^2\approx 4\lambda_D^2/R_p^2$, using $N\approx\pi R_p^2 n$ and $\lambda_D^2\equiv T/4\pi e^2 n$. Thus, the temperature correction is less important when the column is a ''plasma,'' i.e. when $\lambda_D \ll R_p$. In the following section, we compare this formula to experiments.

V. COMPARISON TO EXPERIMENT

We have found that Eq. (24) predicts the measured $m=1$ diocotron frequency to within 5% for columns with lengths $2<L_p/R_w<10$. We find significant deviations for lengths $L_p\lesssim 2R_w$, as would be expected from our approximations. We have varied the column radii over the range $0.25<R_p/R_w<0.73$, and the column temperatures over $0.4\text{ eV}<T<4\text{ eV}$, giving $0.21<\lambda_D/R_p<0.85$.

To obtain columns with different radii, the bias voltage on the filament was varied, with the column radius increasing as the bias becomes more negative. Also, the plasma profile was ''smoothed'' using magnetic tilt transport: the magnetic axis was tilted by $\Delta\theta\sim 10^{-2}$ rad for a few tenths of a second, then re-aligned. This has the effect of ''mixing'' the column, so that it has a more uniform density and temperature. The resulting electron density profile is shown in Fig. 3. It can be seen that the column has nearly uniform density for $r\lesssim 2/3R_p$, with density falling off almost linearly for $r\gtrsim 2/3R_p$. We define R_p to be the point where the density decreases by one half, so that we model the density as the dashed line in the figure. The plasma temperature is also plotted in Fig. 3, and it varies from 1.31 eV to 1.41 eV, with an average of $T=1.35$ eV.

Once the plasma column has been prepared, the diocotron mode is excited by applying electric pulses of opposite sign to two sector probes 180° apart. The pulse duration is short compared to the diocotron period, so the column is driven radially outward. The column then orbits at fixed radius at the diocotron mode frequency. The amplitude of the mode can be varied by changing the duration and amplitude of the pulse.
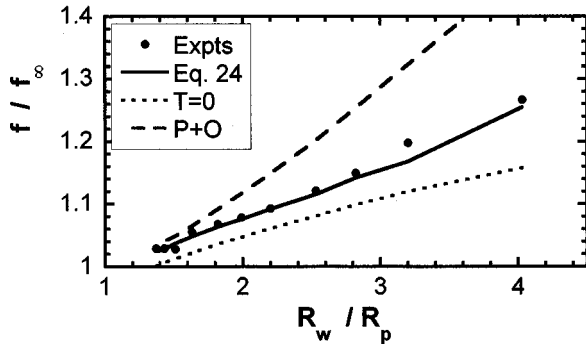
FIG. 4. Measured $m=1$ frequency versus column radius (shown as points), compared to our model Eq. (24) (solid line). Also shown are our model with $T=0$ (dotted line), and the predictions of the theory of Prasad and O'Neil for ''nonrigid'' plasmas[6] (dashed line).
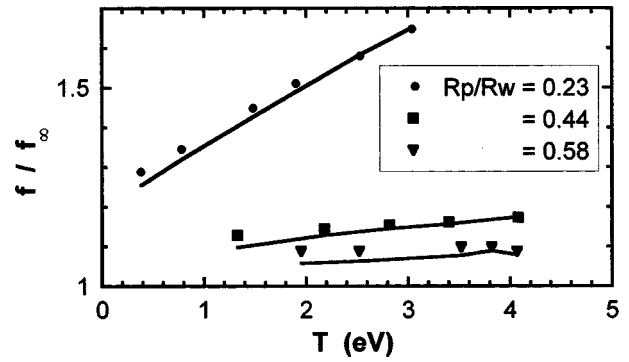

FIG. 5. Measured $m=1$ frequency versus electron temperature, for plasmas with 3 different radii. The model of Eq. (24) is shown by the solid lines.

To obtain the small-amplitude mode frequency, f, a series of measurements are taken at different amplitudes. The finite amplitude frequency, f_A, and amplitude, A, are measured from the received sector probe signal, and 100 shots are averaged at each amplitude. The small amplitude frequency f is then obtained from a fit to $f_A = f(1 + \beta A^2)$, where β and f are fit coefficients.

To measure the number of electrons per unit length, N, we use a Gauss' Law probe. This is simply one cylindrical electrode in the containment region that is connected to an amplifier. When the electrons are dumped axially, a voltage of magnitude Q/C appears on this electrode, where $Q = -eNL_e$, L_e is the electrode length, and C is the electrode capacitance to ground. Care must be taken that this electrode is well away from the column ends, and that the resulting voltage does not trap electrons. The total number of electrons, N_{tot}, is measured by the collimator and collector electrodes, as described previously. The plasma length can then be estimated from $L_p = N_{tot}/N$.

Figure 4 plots the measured (small amplitude) frequencies f/f_∞ versus R_w/R_p, obtained at a magnetic field of 188 G. For these experiments,[10] it is difficult to vary one parameter alone. In Fig. 4, the length changes from 8.3 R_w to 10.2 R_w, and the plasma temperature varies from 0.5 eV to 3.2 eV as R_p is varied. Nevertheless, for each column, we use the measured values of R_p, L_p, N and T in Eq. (24) to calculate the predicted frequency for each experimental point, then connect the calculated points by straight lines. The agreement with the model is quite good, with the biggest discrepancy being 3% of f_∞.

Figure 4 also compares the data to our force-balance model with $T=0$, and to the cold fluid wave-coupling model of Prasad and O'Neil.[7] The $T=0$ curve is substantially below the data, because the thermal pressure on the ends is a significant fraction of the electrostatic pressure: for the narrow, low density plasma with $R_w/R_p = 4$, we obtain $T/Ne^2 = 0.6$. The Prasad and O'Neil wave-coupling theory predicts about twice the measured frequency shifts, and is apparently not applicable for these experiments: the theory implicitly assumes a ''floppy'' plasma with $\nu_b \ll \nu_r$, whereas the experiments are on ''rigid'' plasmas with $\nu_b \gtrsim \nu_r$. The question of whether significant coupling can occur between the

$k_z \approx 0$ diocotron mode and the Landau-damped $k_z \neq 0$ plasma modes could perhaps be addressed with experiments on pure ion plasmas, which tend to be in the floppy regime.

As an erratum, we note that the correspondence suggested by the original comparison[10] of these measurements with the theory of Prasad and O'Neil was erroneous: in Figure 5.5 of Ref. 10, an ''inverted'' length factor was used in calculating the theory, so the displayed theory curve is too low by a factor of $(10R_w/L_p)^2 = (10/8)^2$. Our realization that the theory of Prasad and O'Neil is not applicable to the experimental regime of $\nu_b > \nu_r$ led to development of the present model.

We have also measured the variation of frequency with temperature, as shown in Fig. 5. The temperature is varied by heating the column by alternately compressing and expanding its length for a few cycles.[11] By varying the number of heating cycles, the temperaure can be increased by controlled amounts. Data taken for three different column radii show close agreement with the model, with the largest frequency deviations being 4% of f_∞. The measurements were taken at a magnetic field of 376 G, with column lengths varying from 6.9 R_w to 8.2 R_w.

Finally, we have measured the variation of frequency with column length. This measurement is somewhat more involved than the previous ones. The Gauss' Law technique is not accurate for the shorter lengths, because the measurement electrode must be away from the column ends. Rather, we obtain the length from an (r,z) solution of Poisson's equation with the measured z-integrated charge profile $Q_z(r)$, the measured temperature profile $T(r)$, and the known boundary conditions. To obtain the electron density $n(r,z)$, we assume

$$n(r,z) = n(r,0)\exp[e(\phi(r,z) - \phi(r,0))/T(r)]. \quad (25)$$

In essence, this assumes that the electron plasma is in local thermal equilibrium along each field line. We use a computer code to obtain the self-consistent $n(r,z)$ and $\phi(r,z)$ given the measured $Q_z(r)$, $T(r)$ and wall potentials $\phi(R_w,z)$. Once $n(r,z)$ has been obtained, we define the central line density by $N \equiv \int d^2r \, n(r,z=0)$.

In addition, the magnetic field tilt transport only works for the longest columns, so the short columns must be first
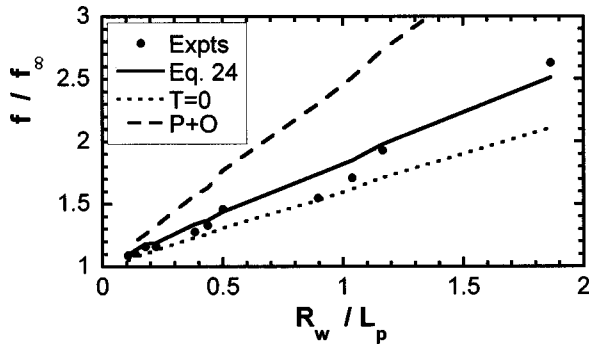
FIG. 6. Measured $m=1$ frequency versus column length (points), compared to our model Eq. (24) (solid line). Also shown are our model with $T=0$ (dotted line), and the predictions of the theory of Prasad and O'Neil for ''nonrigid'' plasmas (Ref. 6) (dashed line).

tilted while long, then cut axially. This cutting process inevitably results in columns that are not as uniform in density as those plotted in Fig. 3.

Figure 6 shows the measured dependence of the diocotron frequency on plasma length L_p. For columns $L_p \geq 2R_w$, the comparison to the present model is good, with the largest variation from the model being about 5% of f_∞. The variation is up to 10% for the shorter length columns. Of course, the model assumes that the columns are long, so that the end confinement fields do not overlap at the axial center. How much of the disagreement comes from the breakdown in the model as compared to the less ''square'' radial profiles is not known.

VI. THE MAGNETRON MODE INCLUDING IMAGE FORCES

There have been a number of experiments in recent years that trap very small ($R_p \ll R_w$) and very short ($L_p \ll R_w$) charge clouds.[12] In this limit, the radial confinement force dominates the $m=1$ orbital motion of the cloud, and the image charge forces are typically not even included in the calculation of the frequency. However, this situation is really just the opposite limit ($L \ll R_w$) of the columns already considered, and the image charge electric fields will appear as additional forces which increase the magnetron frequency. Here, we derive the frequency shift due to these image charges.

Consider a small cloud of electrons contained in cylindrical geometry where the length of the grounded section (B in Fig. 1) is short. Assume that the cloud has total charge $Q = -eN_{\text{tot}}$, and that the cloud is small enough that we can consider it to be a point charge. The confinement potential near the trap center will have the form

$$\phi_c(r,z) = \phi_c(0,0) - \alpha(z^2 - (1/2)r^2), \qquad (26)$$

where the factor of 1/2 in front of r^2 is necessary to satisfy Laplace's equation. The charge cloud orbits the trap axis due to the magnetron motion, and may also oscillate harmonically in z. For a cylindrical wall, the coefficient α can be calculated by expanding $\phi_c(r,z)$ in a Bessel expansion

$$\phi_c(r,z) = -V_c \sum_{n=1}^{\infty} \frac{2}{j_{on}J_1(j_{on})} J_0\left(j_{on}\frac{r}{R_w}\right)$$

$$\times \cosh\left(j_{on}\frac{z}{R_w}\right) e^{-j_{on}L/2R_w}, \qquad (27)$$

where $-V_c$ is the confinement potential at the two ends, and j_{on} is the n-th zero of the J_0 Bessel function. Note that Eq. (27) is only valid in the range $-L/2 < z < L/2$. Near $(r,z) = 0$, the potential behaves as Eq. (26) with

$$\alpha = \frac{V_c}{R_w^2} \sum_{n=1}^{\infty} \frac{j_{on}}{J_1(j_{on})} e^{-j_{on}L/2R_w} \approx 1.15 \frac{V_c}{R_w^2} \frac{L}{R_w}, \qquad (28)$$

where the approximation is valid in the limit $L/R_w \to 0$.

The image charge potential will add to the confinement potential. From symmetry, the images will not result in any net force in the z-direction for uniform radius cylinders, and the harmonic oscillation in z will not be changed. There will be a radial electric field from the image charges, and we calculate this using the part of the Green's function due to images [Eq. (18)]. For a charge Q offset from the axis by distance D, the image potential at $\theta=0$, $z=0$ is

$$\phi_i(r) = \int dz' \int dr' \int r'd\theta' Q\delta(\theta') \frac{\delta(r'-D)}{D}$$

$$\times \delta(z')G_i(x,x')$$

$$\approx -\frac{4}{\pi}Q\int_0^\infty dk\left[\frac{1}{2}\frac{K_0(kR_w)}{I_0(kR_w)}I_0(kr)I_0(kD)\right.$$

$$\left. + \frac{K_1(kR_w)}{I_1(kR_w)}I_1(kr)I_1(kD)\right], \qquad (29)$$

where the approximation is valid to first order in (D/R_w). Using the small argument expansion for I_0 and I_1 we find

$$\phi_i(r) \approx \phi_i(0) - \frac{Q}{\pi}\left[\frac{1}{2}r^2\int_0^\infty dk\ k^2 \frac{K_0(kR_w)}{I_0(kR_w)}\right.$$

$$\left. + rD\int dk\ k^2 \frac{K_1(kR_w)}{I_1(kR_w)}\right], \qquad (30)$$

where $\phi_i(0)$ is a constant.

The integrals can be evaluated numerically to obtain

$$\phi_i(r) \approx \phi_i(0) - \frac{Q}{\pi R_w^3}\left[0.6469\frac{r^2}{2} + 2.5033rD\right]. \qquad (31)$$

Finally, the $m=1$ frequency can be calculated from

$$f = -\frac{cE_r}{2\pi DB} = \frac{c}{2\pi DB}\left[\frac{\partial\phi_c}{\partial r} + \frac{\partial\phi_i}{\partial r}\right]_{r=D}$$

$$= \frac{c}{2\pi B}\left[1.15\frac{V_c}{R_w^2}\frac{L}{R_w} + 1.0027\frac{(-Q)}{R_w^3}\right]. \qquad (32)$$

Here, we see that the confinement force is proportional to V_c, while the image force is proportional to total charge Q, unlike the case of a long column.

This image charge correction may be 1% even for a modest number of charges. As an example, consider 10^5

electrons contained in a trap with $V_c = -10$ Volts, $R_w = 1$ cm and $L/R_w = 0.2$. Using Eq. (32), the frequency due to containment fields is 230 kHz, and the image force term will increase this frequency by 1.4 kHz. As the number of charges is increased, this image correction will become relatively more important, although V_c will eventually have to be increased in order to keep the charges contained.

VII. CONCLUSION

We have presented a model of the $m = 1$ diocotron mode in a finite length column as a rigid displacement of the column, with orbit frequency determined by the sum of the image charge and containment forces. The predicted frequency is in good agreement with measurements for columns longer than about one wall diameter. Experiments also agree with the prediction that the mode frequency increases with plasma temperature. For very short plasmas, we calculate the shift in the magnetron frequency due to image charges.

[1] J. S. DeGrassie and J. H. Malmberg, Phys. Fluids **23**, 63 (1980).
[2] R. C. Davidson, *Physics of Nonneutral Plasmas* (Addison-Wesley, New York, 1990), Sec. 5.6.
[3] L. S. Brown and G. Gabrielse, Rev. Mod. Phys. **58**, 233 (1986).
[4] R. H. Levy, Phys. Fluids **11**, 920 (1968).
[5] K. S. Fine, Phys. Fluids B **4**, 3981 (1992).
[6] N. R. Corngold, Phys. Plasmas **3**, 3324 (1996).
[7] S. A. Prasad and T. M. O'Neil, Phys. Fluids **26**, 665 (1983).
[8] B. P. Cluggish and C. F. Driscoll, Phys. Rev. Lett. **74**, 4213 (1995).
[9] J. D. Jackson, *Classical Electrodynamics*, 2nd edition (Wiley, New York, 1975), p. 118.
[10] K. S. Fine, ''Experiments with the $l = 1$ Diocotron Mode,'' Ph.D. thesis, University of California San Diego (1988).
[11] B. R. Beck, J. Fajans, and J. H. Malmberg, Phys. Rev. Lett. **68**, 317 (1992).
[12] J. J. Bollinger, D. J. Heinzen, F. L. Moore, W. M. Itano, D. J. Wineland, and D. H. E. Dubin, Phys. Rev. A **48**, 525 (1993).